Analytic solutions for the stress field in static sandpiles

M. Angelillo[a,*], E. Babilio[b], A. Fortunato[a], M. Lippiello[b], A. Montanino[c]

[a] *Department of Civil Engineering, University of Salerno, Via Ponte Don Melillo, Fisciano 84084, SA, Italy*
[b] *Department of Structures for Engineering and Architecture, University of Naples "Federico II", Via Forno Vecchio 36, Napoli 80134, Italy*
[c] *Centro di Simulazione Numerica Avanzata (CeSNA), Istituto Universitario di Studi Superiori (IUSS), Pavia, Italy*

A B S T R A C T

In the present paper we propose a new class of analytical solutions for the equilibrium problem of a prismatic sand pile under gravity, capturing the effects of the history of the sand pile formation on the stress distribution. The material is modeled as a continuum composed by a cohesionless granular material ruled by Coulomb friction, that is a material governed by the Mohr–Coulomb yield condition. The closure of the balance equations is obtained by considering a special restriction on stress, namely a special form of the stress tensor relative to a special curvilinear, locally non-orthogonal, reference system.

This assumption generates a class of closed-form equilibrium solutions, depending on three parameters. By tuning the value of the parameters a family of equilibrium solutions is obtained, reproducing closely some published experimental data, and corresponding to different construction histories, namely, for example, the deposition from a line source and by uniform raining. The repertoire of equilibrated stress fields that we obtain in two special cases contains an approximation of the *Incipient Failure Everywhere* (IFE) solution and a closed-form description of the arching phenomenon.

1. Introduction

Granular piles in static equilibrium have attracted much interest due to their rich physical phenomenology and the number of curious effects that they exhibit. The most popular among these effects is the appearance of a stress dip at the center of the pile, that was detected experimentally and described and interpreted by several papers in the late 1990s . The main result of these studies (among which we recall the comprehensive work of Wittmer et al. (1996) and the extensive references cited therein) is that the dip is a result of arching. Describing the degree of arching and predicting its dependence on the construction history was, at that time, still an open issue.

Such a challenge was taken up lately by a number of researchers, among which we recall Michalowski and Park (2004a, 2004b); 2005), Pipatpongsa and Siriteerakul (2010), Pipatpongsa et al. (2010), which propose some analytic stress solutions, and Bierwisch et al. (2009), Sibille et al. (2015) and Zhu et al. (2008), which adopt numerical approaches based on discrete element simulations.

In the present paper we propose a new analytical solution to the equilibrium problem of a prismatic sand pile under gravity. Our main objective is to give closed-form solutions of the equilibrium equations, capable of describing the different degrees of arching that are determined by different construction histories. It is a fact, for example as shown by Vanel et al. (1999), that the pressure dip beneath the pile can have different profiles or even almost disappear depending on the loading history. Such an effect is

* Corresponding author. Tel.: +39 089964073; fax: +39 089964045.
E-mail addresses: mangelillo@unisa.it (M. Angelillo), enrico.babilio@unina.it (E. Babilio), a.fortunato@unisa.it (A. Fortunato), maria.lippiello@unina.it (M. Lippiello), andrea.montanino@iusspavia.it (A. Montanino).

captured by our closed-form solution just by tuning three parameters.

The material is modeled as a continuum composed by a cohesionless granular material. The modeling strategy is based on some simplifying assumptions:

- There is a stress tensor $\mathbf{T}$ which is well defined as a local average over many grains.
- The particle are hard (that is are rigid), therefore no elastic strain variable exists and the static frictional forces are indeterminate.
- Friction is ruled by Coulomb linear law, that is the stress is restricted by inequalities depending on a single coefficient (see the inequalities (2) below).
- The construction history determines the grain arrangement and packing, that is the local restrictions ruling the stress.

In the model there is no trace of elasticity or of any constitutive behaviour or dependence of the stress on the strain or on the strain rate. The main tool that we use to select a particular equilibrium solution is represented by the choice of a special curvilinear system (θ_1, θ_2), with the lines θ_2 directed vertically and the lines θ_1 directed along curved trajectories. This family of curved lines can be chosen, in principle, in an infinite number of different ways, but we explore just the easiest possibilities namely: hyperbolas and parabolas. The closure condition that we adopt to make the problem statically determined, consists in assuming that the tangential stress component, in this special reference system, is zero, that is the vertical load (the body load) is taken by normal stresses directed as the vertical lines θ_2 and as the curved lines θ_1. The ratio between the load that is taken by the columns, and the load that is taken by the arches can be regulated by tuning three parameters.

In particular, in the case in which the curved lines are parabolas, we find two special solutions that, in terms of base pressures, resemble closely the experiments by Vanel et al. (1999).

2. The Coulomb friction model

As a first approximation to the behaviour of dry granular masses, a cohesionless material ruled by Coulomb friction, that is a material governed by the Mohr–Coulomb yield condition, can be adopted. This crude unilateral model material that idealizes the real material as indefinitely strong if compressed within the yield cone, but incapable of sustaining stresses outside the yield surface, is perfectly rigid in compression, in the sense that no strain rates can occur if the stress is inside the limit surface. The material can exhibit unaccelerated flow when the stress belongs to the limit surface and accelerated motion must occur if the stress is outside the yield locus (see Lippiello, 2007).

If we restrict to statics, and exclude therefore the possibility of accelerated motion, the stress state is restricted to belong to the Mohr–Coulomb cone. In the plane case, denoting $\mathbf{T}$ the stress tensor, the Mohr–Coulomb restriction, in terms of the first and second stress invariants

$$\iota_1(\mathbf{T}) = \operatorname{tr}\mathbf{T} \quad \iota_2(\mathbf{T}) = \det\mathbf{T}, \tag{1}$$

can be written as follows:

$$\det\mathbf{T} - \cos^2(\varphi)\left(\frac{\operatorname{tr}\mathbf{T}}{2}\right)^2 \geq 0\,, \quad \operatorname{tr}\mathbf{T} \leq 0, \tag{2}$$

φ being the friction angle.

With Coulomb friction there is a linear relation between the normal component of stress and the maximum admissible tangential component that can be exerted on a given surface. When shear stress reaches this maximum value sliding on that surface becomes possible. Such a sliding is geometrically similar to the slipping occurring along discontinuity lines (concentrated shearing) in some perfectly plastic metallic materials, say plastic materials governed by the Mises yield condition. Energy is dissipated into heat during flow in both cases.

Unfortunately whilst the slipping flow rule of Mises materials is associative, the slipping of a Mohr–Coulomb material is not, since, for any value of the friction angle φ in the open interval $(0, \pi)$, such a strain rate is not orthogonal to the limit surface. Therefore the statics of frictional materials cannot be treated within the frame of Limit Analysis, unless the friction angle is $\pi/2$ (No-Tension materials, see Heyman, 1966; Angelillo, 1993; Fortunato, 2010; Angelillo et al., 2010, 2014a, 2014b, 2014c) or 0 (perfect unilateral fluids, see Chorin and Marsden, 2000; Dostal, 2009; Schechter and Bridson, 2012).

This means that, if, for a given structure under given loads, we find a stress field that is equilibrated with the loads and within the yield limits (that is a *statically admissible* stress field), we are not sure that the same structure, under the same loads, would not collapse for some special loading histories.

In the application we present here, we focus on the statical approach, namely, on assuming some closure restrictions on stress, we obtain statically admissible stress fields, that, in principle, can be attained by performing special loading histories. Actually, for granular masses the loading history is determined by the construction history, which determines the arrangement of *grains* and, therefore, the way in which the grains interact, that is, in the continuum model, the special material restrictions that are locally valid.

3. Formulation of the problem

The equilibrium of a prismatic sand pile of height h and base $2a$ (Fig. 1), and standing on a perfectly rigid rough plane, is considered. The angle of repose $\psi = \arctan(h/a)$ of the pile is usually assumed coincident with the friction angle of the material φ, though the case of a repose angle less than φ can be considered.

The typical construction history for a prismatic sand pile consists in pouring the material from a *line source*. Another typical construction history considers the pile constructed through uniform deposition (*uniform raining*).

3.1. Geometry and curvilinear coordinates

The relevant geometrical dimensions of a prismatic pile are its height h and its width $2a$. By reducing the problem to the plane case, the density ρ of the material is defined

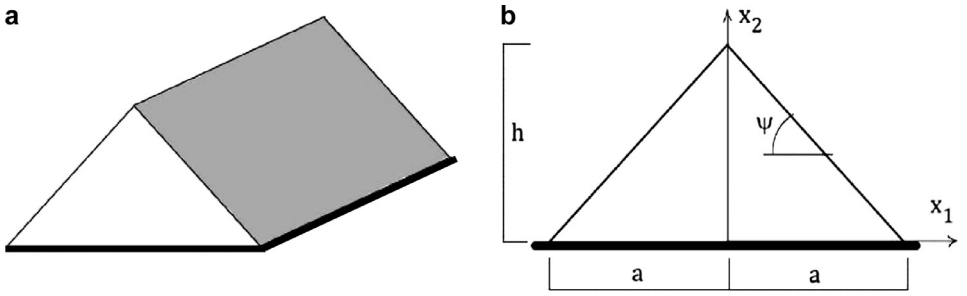

Fig. 1. Perspective view of a prismatic sand pile in planar equilibrium (a). Cross section and relevant notation (b).

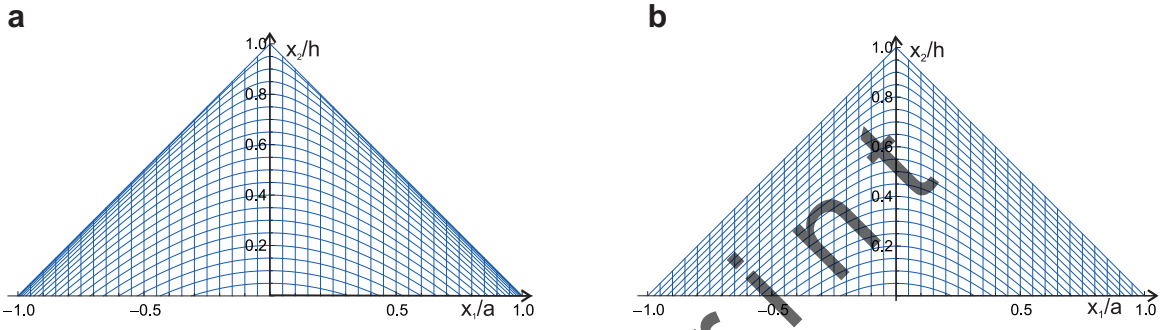

Fig. 2. Forms A and B of the function f(a) plotted as a function of θ_1, for $\theta_2 = const$. form A in (a), form B in (b).

per unit area, and the stress is a generalized stress (that is a force per unit length). A schematic perspective view of a sand pile supported on a rigid base is depicted in (Fig. 1a).

For simplicity, the density of the material, actually variable along the height due to the changing porosity of the material on moving from the free surface to the base, is considered as a constant.

By denoting {...} the components of vector quantities with respect to the Cartesian frame shown in (Fig. 1b), the special curvilinear coordinate system (θ_1, θ_2) defined through the relations

$$\mathbf{x}(\theta_1, \theta_2) = \{\theta_1, f(\theta_1, \theta_2)\} \tag{3}$$

is introduced to describe the problem. In (3) the function f is a generic smooth function of θ_1, θ_2, even with respect to θ_1, strictly monotonic with respect to θ_2, and such that

$$f(\theta_1, 0) = h - \frac{h}{a}|\theta_1| \qquad f(0, a) = 0. \tag{4}$$

In particular, we assume that $\theta_1 \in [-a, a]$ and restrict to the values of $\theta_2 \in [0, a]$ such that $\mathbf{x}$ is into the sand pile, that is belongs to the triangular domain Ω comprised from the pile free surface and the rigid base.

A typical arrangement of the curvilinear lines θ_1, described at $\theta_2 = const$, by hyperbolas (that is sections of a circular cone, centered at the vertex of the pile, with planes parallel to the cone axis) is shown in Fig. 2a.

The idea behind the choice of this special curvilinear system is better clarified by the closure assumption that we make later, to render the equilibrium problem statically determined. All we can say here is that, with our assumption, the self-load is carried partly by elementary columns delimited by two closely spaced vertical lines θ_2, and partly by elementary arches delimited by two closely spaced curved lines θ_1.

The natural (covariant) base vectors associated to the curvilinear system defined on S by the couple (θ_1, θ_2), are

$$\mathbf{a}_1 = \{1, f_{,1}\},$$
$$\mathbf{a}_2 = \{0, f_{,2}\}, \tag{5}$$

where a comma followed by an index, say α, stands for differentiation with respect to x_α.

The reciprocal (contravariant) base vectors are

$$\mathbf{a}^1 = \{1, 0\},$$
$$\mathbf{a}^2 = \left\{\frac{-f_{,1}}{f_{,2}}, \frac{1}{f_{,2}}\right\}. \tag{6}$$

The basic elements of differential geometry, necessary to render this analysis self-contained, are summarized in Appendix A.

3.2. Equilibrium

The generalized stress in Ω, is defined by the stress tensor $\mathbf{T}$. In the covariant base, by adopting summation convention on repeated Greek indexes, $\alpha, \beta, \gamma, \ldots = 1, 2$, it can be represented as follows

$$\mathbf{T} = T^{\alpha\beta}\mathbf{a}_\alpha \otimes \mathbf{a}_\beta, \tag{7}$$

$T^{\alpha\beta}$ being the contravariant components of $\mathbf{T}$. Notice that the basis $(\mathbf{a}_1, \mathbf{a}_2)$ is neither unit nor orthogonal, then though the contravariant components are useful and convenient, they are *non-physical* components of stress, and a bit of conversions is needed to transform them into Cartesian stress components.

Internal equilibrium is dictated by the condition that the divergence of the generalized surface stress $\mathbf{T}$ balances the load $\mathbf{b} = \{0, -\rho g\}$, defined per unit area on Ω. Such a vector/differential condition can be written, explicitly, as follows (see Appendix A)

$$\frac{\partial}{\partial \theta_\gamma}(T^{\alpha\beta}\mathbf{a}_\alpha \otimes \mathbf{a}_\beta)\mathbf{a}^\gamma + \mathbf{b} = \mathbf{0}. \tag{8}$$

Indeed, by projecting Eq. (7) into the two non-collinear directions $\mathbf{a}^1$, $\mathbf{a}^2$, after some simple transformations (and considering that $f_{,2}$ is never zero by assumption) one obtains

$$\begin{aligned}&(T^{11}f_{,2})_{,1} + (T^{12}f_{,2})_{,2} = 0,\\ &(T^{12}f_{,2}{}^2)_{,1} + (T^{22}f_{,2}{}^2)_{,2} + T^{12}f_{,2}f_{,12}\\ &\quad + T^{11}f_{,2}f_{,11} - \rho g f_{,2} = 0.\end{aligned} \tag{9}$$

We consider traction boundary conditions at the free surface that is

$$\mathbf{T}(\theta_1, 0)\mathbf{n} = \mathbf{0}, \tag{10}$$

$\mathbf{n}$ being the unit outward normal to the free surface. Taking into account the material restrictions (2), that is the fact that the material is strictly unilateral, the stress itself must vanish at the free surface, and we obtain three scalar conditions:

$$T^{11}(\theta_1, 0) = 0, \quad T^{12}(\theta_1, 0) = 0, \quad T^{22}(\theta_1, 0) = 0. \tag{11}$$

3.3. Closure assumption

The *closure* restriction on stress that we assume is that the stress component T^{12} in this special reference system is zero everywhere in Ω. With this assumption we consider that the load due to gravity is balanced in part by a vertical normal stress component, and, for another part, by a normal stress tangent to the arch-like curvilinear lines $\theta_2 = const$, defined by the function f.

Then the system (8) is closed and we may integrate it to find the two non-vanishing stress components T^{11} and T^{22}.

On assuming $T^{12} = 0$, the equilibrium equations (8) reduce to the form

$$\begin{aligned}&(T^{11}f_{,2})_{,1} = 0,\\ &(T^{22}f_{,2}{}^2)_{,2} = -T^{11}f_{,2}f_{,11} + \rho g f_{,2},\end{aligned} \tag{12}$$

where f is a given function, to be integrated with the following boundary conditions:

$$T^{11}(\theta_1, 0) = 0\,, \quad T^{22}(\theta_1, 0) = 0. \tag{13}$$

3.4. A restricted family of balanced stress fields

The form of the solution that we obtain depends on the choice of the form of f. Of course, if we accept numerical solutions, there exist an endless repertoire of possible functions f that could be explored. In the present paper, confining ourselves to analytical solutions, we consider only the simplest choices, namely the forms A and B:

$$f^A = h - \frac{h}{a^2}\sqrt{r^2 - a^2} - \frac{h}{a^2}\sqrt{a^2\theta_1^2 + r^2\theta_2^2},$$

$$f^B = -\frac{h}{2a}\left(\theta_2 + \sqrt{4\theta_1^2 + \theta_2^2} - 2a\right), \tag{14}$$

shown graphically in Fig. 2a and b, for comparison. Forms A and B can be produced by interesting cones based on the triangular domain Ω (in the sense that the vertex of the cone coincides with the vertex $\{0, h, 0\}$ of the triangle, and the slanted sides of the triangle are two of the generating half-lines of the cone) with planes parallel to the plane of Ω, that is orthogonal to the axis x_3 perpendicular to $(O; x_1, x_2)$. Form A is obtained by considering as the diretrix curve a circle of radius r contained in the plane $(O; x_3, x_1)$ and passing through the points $\{-a, 0, 0\}$, $\{a, 0, 0\}$. Form B is obtained by considering as the diretrix curve a parabola contained in the plane $(O; x_3, x_1)$ and passing through the points $\{-a, 0, 0\}$, $\{o, a, 0\}$, $\{a, 0, 0\}$. Forms A (in the special case $r = a$) and B are reported pictorially in Fig. 2.

On integrating the first of Eqs. (12) one obtains

$$T^{11} = \frac{m(\theta_2)}{f_{,2}}, \tag{15}$$

$m(\theta_2)$ being an unknown numeric function of θ_2, that we develop in a power series retaining the cubic terms only:

$$m(\theta_2) = k_0 + k_1\theta_2 + k_2\theta_2^2 + k_3\theta_2^3. \tag{16}$$

At this point we have to choose the more convenient form of f. In the present paper we have exploited the most elementary choice, namely $f = f^B$. This choice leads easily, as we shall see, to a closed-form representation of a restricted class of equilibrated stress field depending on three parameters. The different experiments we made with the form f^A, corresponding to different choices of r (though limited in number), were not successful. In particular the form f^A, for $r = a$, cannot be used since $f_{,2}$ diverges for $r \to a$. The other choices of r that we tested produce stresses that are not admissible, in the sense that do not satisfy the Mohr–Coulomb inequalities (2) for any value of the three parameters, within the sand pile.

On assuming for f the form B, since

$$f_{,2} = -\frac{h}{2a}\left(1 + \frac{\theta_2}{\sqrt{4\theta_1{}^2 + \theta_2{}^2}}\right), \tag{17}$$

the first boundary condition on the stress gives $k_0 = 0$, that is

$$T^{11}f_{,2} = m(\theta_2) = k_1\theta_2 + k_2\theta_2^2 + k_3\theta_2^3, \tag{18}$$

and then

$$T^{11} = -\frac{2a\theta_2\sqrt{4\theta_1^2 + \theta_2^2}\left(k_1 + k_2\theta_2 + k_3\theta_2^2\right)}{h\left(\theta_2 + \sqrt{4\theta_1^2 + \theta_2^2}\right)}. \tag{19}$$

Taking into account (18), from the second of Eq. (12), one obtains

$$T^{22}f_{,2}^2 = \int \left(\rho g f_{,2} - \left(k_1\theta_2 + k_2\theta_2^2 + k_3\theta_2^3\right)f_{,11}\right)\mathrm{d}\theta_2. \tag{20}$$

Recalling Eq. (17) and taking into account that for the form B of f

$$f_{,1} = -\frac{2h\theta_1}{a\sqrt{4\theta_1^2 + \theta_2^2}},$$

$$f_{,11} = -\frac{2h\theta_2^2}{a\left(4\theta_1^2+\theta_2^2\right)^{3/2}}, \tag{21}$$

one obtains

$$\begin{aligned} T^{22} f_{,2}^2 &= \frac{gh\rho}{2a}\left(2a-\theta_2-\sqrt{4\theta_1^2+\theta_2^2}\right) \\ &+ \frac{2h}{a}\left(-6k_2\log\left(\theta_2+\sqrt{4\theta_1^2+\theta_2^2}\right)\theta_1^2+\frac{48k_1\theta_1^2-256k_3\theta_1^4}{12\sqrt{\theta_1^2}}\right) \\ &+ n(\theta_1), \end{aligned} \tag{22}$$

$n(\theta_1)$ being an unknown numeric function of θ_1.

On imposing the second of the boundary conditions (13), one finally obtains

$$\begin{aligned} T^{22} f_{,2}^2 &= -\frac{gh\rho}{2a}\left(2a-2\sqrt{\theta_1^2}\right) \\ &- \frac{2h}{a}\left(-6k_2\log\left(2\sqrt{\theta_1^2}\right)\theta_1^2+\frac{48k_1\theta_1^2-256k_3\theta_1^4}{12\sqrt{\theta_1^2}}\right) \\ &+ \frac{gh\rho}{2a}\left(2a-\theta_2-\sqrt{4\theta_1^2+\theta_2^2}\right) - \frac{2h}{a}\left(\frac{k_2\log\left(\theta_2+\sqrt{4\theta_1^2+\theta_2^2}\right)\theta_1^2}{\sqrt{4\theta_1^2+\theta_2^2}}\right) \\ &+ \frac{2h}{a}\left(\frac{6k_1\left(8\theta_1^2+\theta_2^2\right)+3k_2\theta_2\left(12\theta_1^2+\theta_2^2\right)-2k_3\left(128\theta_1^4+16\theta_1^2\theta_2^2-\theta_2^4\right)}{6\sqrt{4\theta_1^2+\theta_2^2}}\right). \end{aligned} \tag{23}$$

The physical stress components, denoted $T_{(\alpha\beta)}$, and representing the Cartesian components of stress in the given Cartesian frame $(O; x_1, x_2)$, can be obtained from the contravariant components $T^{\alpha\beta}$ through the formula

$$T_{(\alpha\beta)} = \left(T^{\mu\nu}\mathbf{a}_\mu\otimes\mathbf{a}_\nu\right)\cdot\hat{\mathbf{e}}_\alpha\otimes\hat{\mathbf{e}}_\beta, \tag{24}$$

where $\hat{\mathbf{e}}_\alpha$ are the unit base vectors associated to the Cartesian frame $(O; x_1, x_2)$, that is, with the notation adopted for Cartesian components in the global frame, $\hat{\mathbf{e}}_1 = \{1, 0\}$, $\hat{\mathbf{e}}_2 = \{0, 1\}$.

In particular, recalling (5) and (6), one has

$$\begin{aligned} T_{(11)} &= \left(T^{11}\mathbf{a}_1\otimes\mathbf{a}_1+T^{22}\mathbf{a}_2\otimes\mathbf{a}_2\right)\cdot\hat{\mathbf{e}}_1\otimes\hat{\mathbf{e}}_1 = T^{11}, \\ T_{(12)} &= \left(T^{11}\mathbf{a}_1\otimes\mathbf{a}_1+T^{22}\mathbf{a}_2\otimes\mathbf{a}_2\right)\cdot\hat{\mathbf{e}}_1\otimes\hat{\mathbf{e}}_2 = T^{11}f_{,1}, \\ T_{(22)} &= \left(T^{11}\mathbf{a}_1\otimes\mathbf{a}_1+T^{22}\mathbf{a}_2\otimes\mathbf{a}_2\right)\cdot\hat{\mathbf{e}}_2\otimes\hat{\mathbf{e}}_2 \\ &= T^{11}f_{,1}^2+T^{22}f_{,2}^2, \end{aligned} \tag{25}$$

that is

$$\begin{aligned} T_{(11)} &= -\frac{2a\theta_2\sqrt{4\theta_1^2+\theta_2^2}\left(k_1+k_2\theta_2+k_3\theta_2^2\right)}{h\left(\theta_2+\sqrt{4\theta_1^2+\theta_2^2}\right)}, \\ T_{(12)} &= \frac{4\left(k_1+k_2\theta_2+k_3\theta_2^2\right)\theta_1\theta_2}{\theta_2+\sqrt{4\theta_1^2+\theta_2^2}}, \\ T_{(22)} &= -\frac{gh\rho}{2a}\left(2a-2\sqrt{\theta_1^2}\right) \\ &+ \frac{2h}{a}\left(6k_2\log\left(4\sqrt{\theta_1^2}\right)\theta_1^2-\frac{48k_1\theta_1^2-256k_3\theta_1^4}{12\sqrt{\theta_1^2}}\right) \\ &+ \frac{gh\rho}{2a}\left(2a-\theta_2-\sqrt{4\theta_1^2+\theta_2^2}\right) \\ &- \frac{2h}{a}\left(\frac{4\theta_1^2\theta_2\left(k_1+k_2\theta_2+k_3\theta_2^2\right)}{\sqrt{4\theta_1^2+\theta_2^2}\left(\theta_2+\sqrt{4\theta_1^2+\theta_2^2}\right)}\right) \\ &- \frac{2h}{a}\left(\frac{k_2\log\left(2\left(\theta_2+\sqrt{4\theta_1^2+\theta_2^2}\right)\right)\theta_1^2}{\sqrt{4\theta_1^2+\theta_2^2}}\right) \\ &+ \frac{2h}{a}\left(\frac{6k_1\left(8\theta_1^2+\theta_2^2\right)+3k_2\theta_2\left(12\theta_1^2+\theta_2^2\right)+2k_3\left(-128\theta_1^4-16\theta_1^2\theta_2^2+\theta_2^4\right)}{6\sqrt{4\theta_1^2+\theta_2^2}}\right). \end{aligned} \tag{26}$$

The stress fields described by expression (26) define a class of equilibrated solutions depending on the three parameters k_1, k_2 and k_3. By choosing $\{k_1, k_2, k_3\}/(\rho g)$ in the interval $\Gamma = \{[0, 1], [-1, 1], [0, 1]\}$, a family of stress fields is obtained whose admissibility, in the sense of the Mohr–Coulomb condition (2), has to be verified.

For example, by taking $k_1 = k_2 = k_3 = 0$, a compressive, uniaxial vertical stress field is obtained, and the stress is statically admissible only if the friction angle of the material is $\pi/2$. By taking $\{k_1, k_2, k_3\}/(\rho g)$ in the range Γ, a compressive biaxial stress field is obtained and the admissibility of the stress must be verified by checking that inequality (2), that is, in components form

$$T_{(11)}T_{(22)} - T_{(12)}^2 - \cos^2(\varphi)\left(\frac{T_{(11)}+T_{(22)}}{2}\right)^2 \geq 0, \tag{27}$$

is satisfied.

To look at the admissibility of the equilibrated stress states that we produce, and measure their degree of safeness, we introduce the non-dimensional distance

$$d(\mathbf{T}) = \frac{\det\mathbf{T}}{\left(\frac{\mathrm{tr}\,\mathbf{T}}{2}\right)^2} - \cos^2(\varphi), \tag{28}$$

defined for any $\mathbf{T}$ such that $\mathrm{tr}\,\mathbf{T} < 0$. Such a distance is positive, and has actually a maximum for $\mathbf{T} = \sigma\mathbf{I}$ $(\sigma > 0)$, of value $d(-\sigma\mathbf{I}) = 1 - \cos^2(\varphi)$; $d(\mathbf{T})$ is positive if $\mathbf{T}$ is safe, is zero when $\mathbf{T}$ is a yield state, and becomes negative when $\mathbf{T}$ is outside the cone.

4. A simple example

4.1. First case: $\psi = 45^\circ$, $\varphi = 45^\circ$, $k_1 = 0.1287\ \rho g$, $k_2 = k_3 = 0$

To fix ideas we first consider the case in which $a = h$, that is the angle of repose $\psi = 45^\circ$, and the friction angle φ coincides with ψ. By assuming $k_2 = k_3 = 0$ and changing the value of the parameter k_1 in the range [0, 1] we find that the stress satisfies the Mohr Coulomb constraint, in a narrow neighborhood around a single value of k_1, namely $k_1 = 0.12827\ \rho g$. The results in terms of stress, corresponding to such a choice are summarized in Figs. 3–5, in a scale normalized by taking $\rho g = 1$, $a = 1$. In particular, in Fig. 3 the contour plot of the physical stress component $T_{(11)}$ is reported. Analogous plots of the shear component $T_{(12)}$ and of the normal component $T_{(22)}$ are depicted in Figs. 4 and 5.

In Fig. 9a, the contour plot of the distance $d(\mathbf{T})$ introduced in (28) is represented. From such a plot we see that the yield function is strictly positive all over the triangular domain, though the value of it is rather small being less than 10^{-3}, all over the domain. This means that the

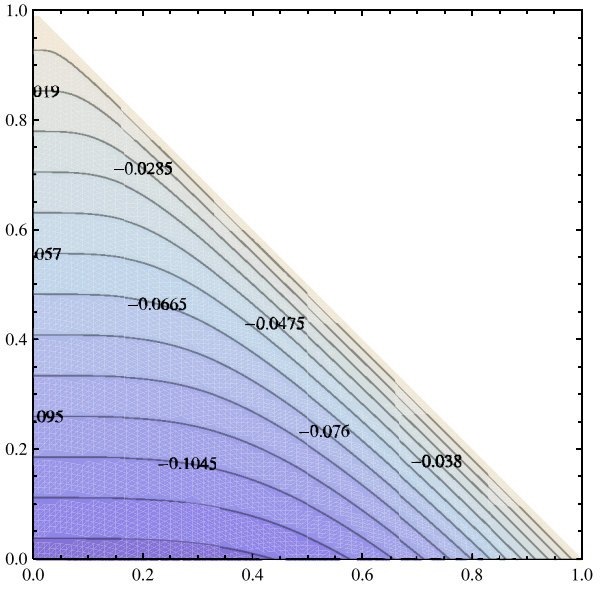

Fig. 3. Physical stress component $T_{(11)}$ as a function of θ_1, θ_2, for the first example: $\psi = 45^\circ$, and $\varphi = 45^\circ$. Contour plot of $T_{(11)}$ in the right hand side of the pile.

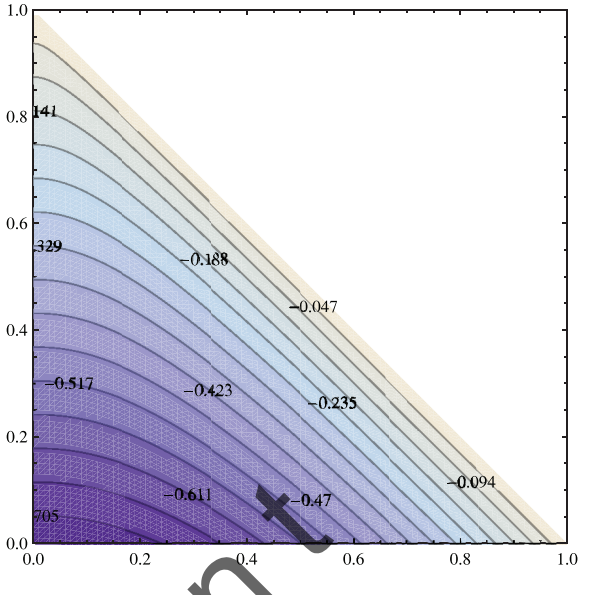

Fig. 5. Physical stress component $T_{(22)}$ as a function of θ_1, θ_2, for the first example: $\psi = 45^\circ$, and $\varphi = 45^\circ$. Contour plot of $T_{(22)}$ in the right hand side of the pile.

stress is very close to the limit surface that is close to the limit state at each point of Ω; therefore the equilibrium is highly unstable and such stress state can be maintained only admitting a very careful and smooth construction history. Any small vibration of the base of the pile or any other energy input from the outside due to an outside disturbance, would produce a sudden loss of stability with a small change of the profile of the pile and a corresponding loss of potential energy, at the price of interface frictional energy (heat).

In Fig. 10a the profile of the stresses $T_{(22)}$, $T_{(12)}$, and of the stress component $T_{(11)}$, emerging at the base of the pile is depicted. Notice that we adopted the sign convention for stress in the stress matrix, then the negative sign of the normal stress means that $T_{(22)}$ points upward, and the positive sign of the shear stress means that $T_{(12)}$ points toward the left.

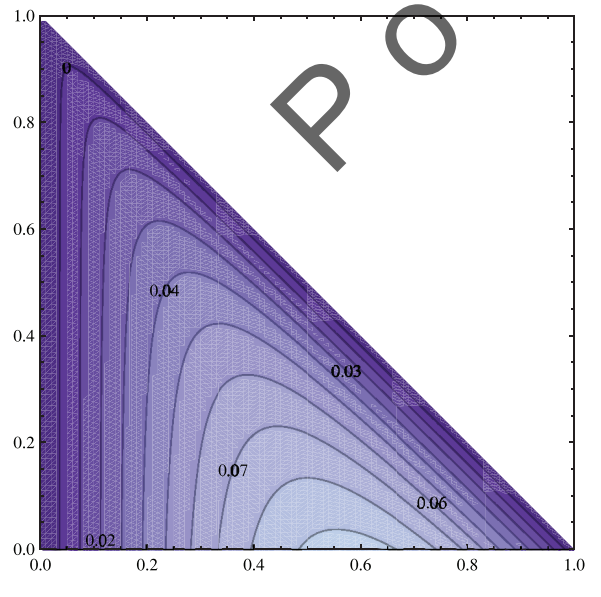

Fig. 4. Physical stress component $T_{(12)}$ as a function of θ_1, θ_2, for the first example: $\psi = 45^\circ$, and $\varphi = 45^\circ$. Contour plot of $T_{(12)}$ in the right hand side of the pile.

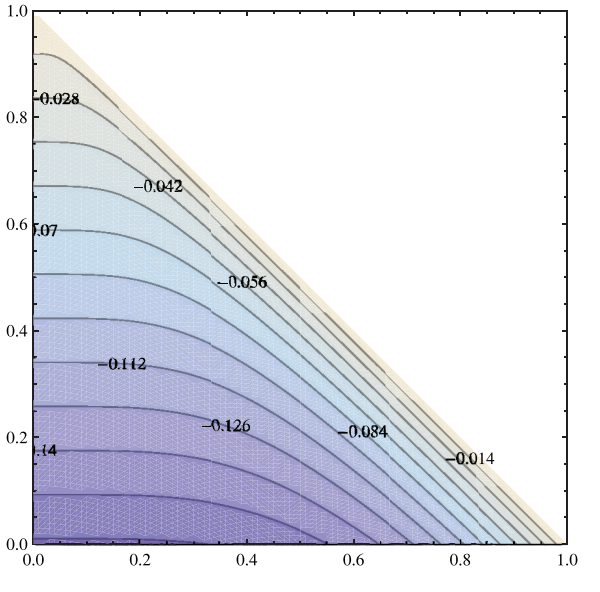

Fig. 6. Physical stress component $T_{(11)}$ as a function of θ_1, θ_2, for the second example: $\psi = 45^\circ$, and $\varphi = 46^\circ$. Contour plot of $T_{(11)}$ in the right hand side of the pile.

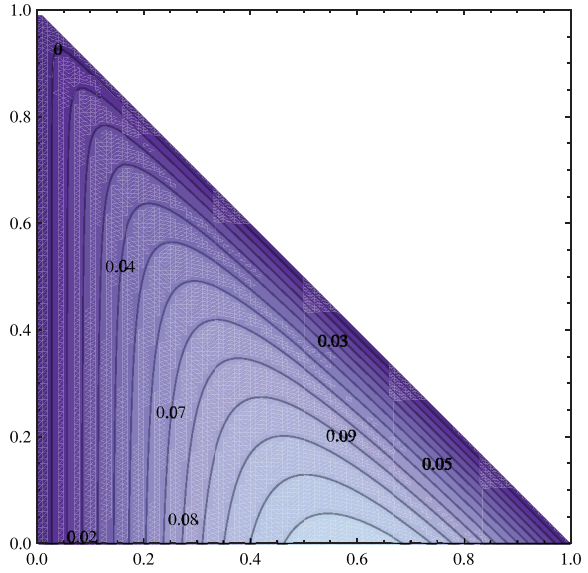

Fig. 7. Physical stress component $T_{(12)}$ as a function of θ_1, θ_2, for the second example: $\psi = 42^\circ$, and $\varphi = 46^\circ$. Contour plot of $T_{(12)}$ in the right hand side of the pile.

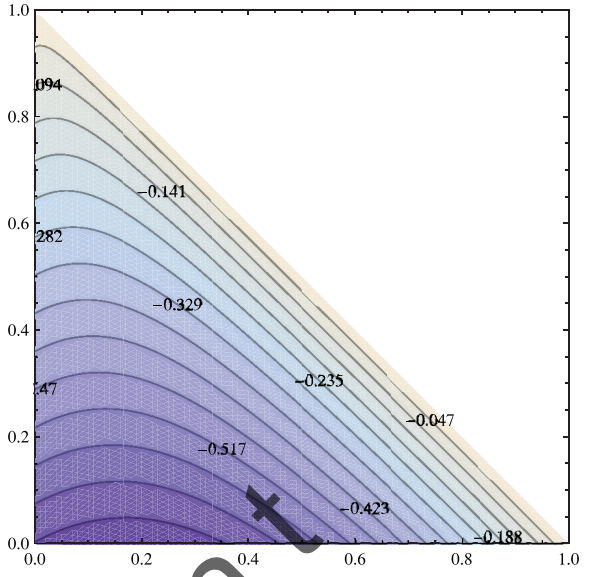

Fig. 8. Physical stress component $T_{(22)}$ as a function of θ_1, θ_2, for the second example: $\psi = 45^\circ$, and $\varphi = 46^\circ$. Contour plot of $T_{(22)}$ in the right hand side of the pile.

4.2. Second case: $\psi = 45^\circ$, $\varphi = 46^\circ$, $k_1 = 0.19\ \rho g$, $k_2 = k_3 = 0$

As a second case, we then consider $h = \arctan 45^\circ$, namely that the angle of repose is $\psi = 45^\circ$, whilst we assume for the friction angle $\varphi = 46^\circ$. The idea is that the pile has suffered a less smooth construction history, with the result that the angle of repose is less than the friction angle. By assuming $k_2 = k_3 = 0$ and changing the value of the parameter k_1 in the range [0, 1] we find that the stress satisfies the Mohr Coulomb constraint, over an interval of values of k_1, whose maximum is $k_1 = 0.17\ \rho g$. The results in terms of stress, corresponding to such a choice are summarized in Figs. 6–8 in a scale normalized by taking $\rho g = 1$, $a = 1$. In particular in Fig. 6 the 3d plot and the contour plot of the physical stress component $T_{(11)}$ is reported. Analogous plots of the normal component $T_{(12)}$ and of the shear component $T_{(22)}$ are depicted in Figs. 7 and 8.

In Fig. 9b, the contour plot of the distance $d(\mathbf{T})$ is represented. From such a plot we see that the yield function is

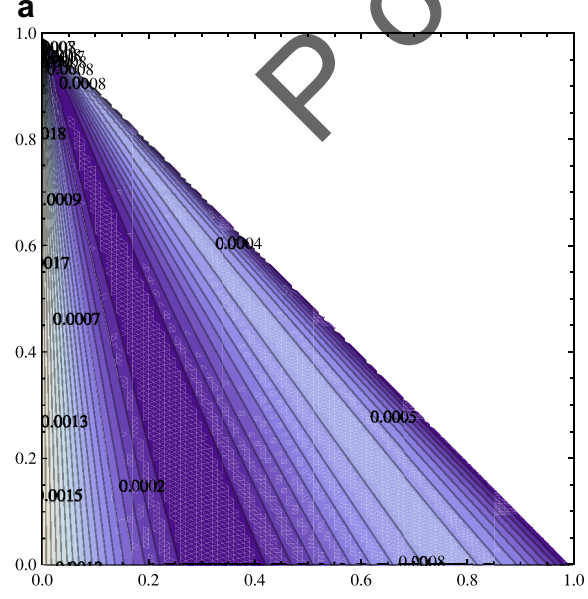

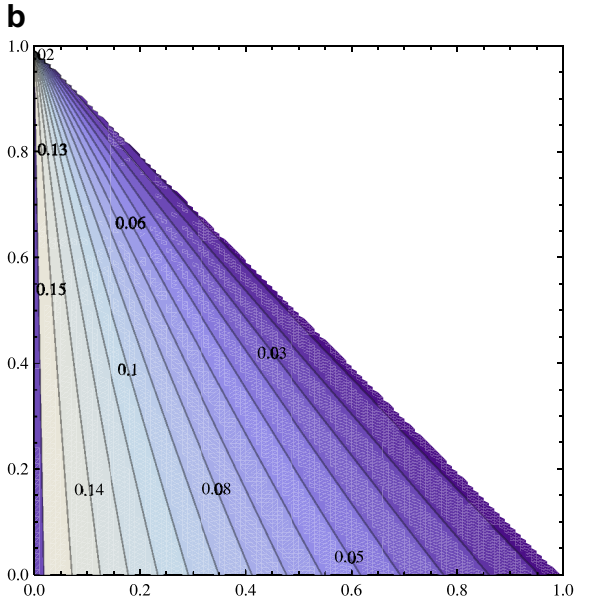

Fig. 9. Contour plot of $g = 1 - \cos^2(\varphi)(\mathrm{tr}\mathbf{T}/2)^2/\det\mathbf{T}$ as function of θ_1, θ_2, for the first (a) and the second (b) examples.

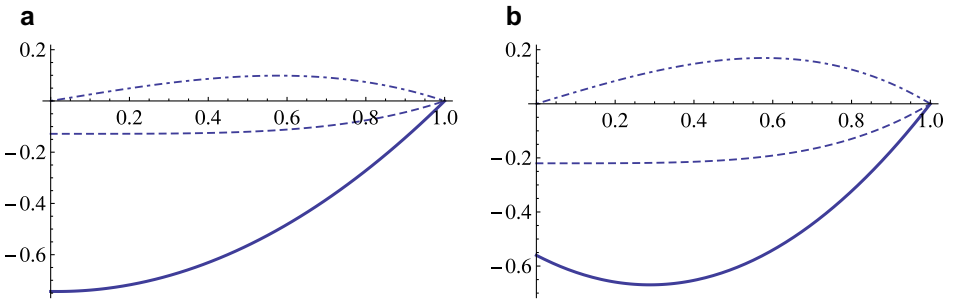

Fig. 10. Plot of the stress profiles at the base for the first (a) and the second (b) examples as functions of x_1, in the interval [0, a]. Dotted-dashed line: $T_{(12)}$, dashed line: $T_{(11)}$, solid line: $T_{(22)}$.

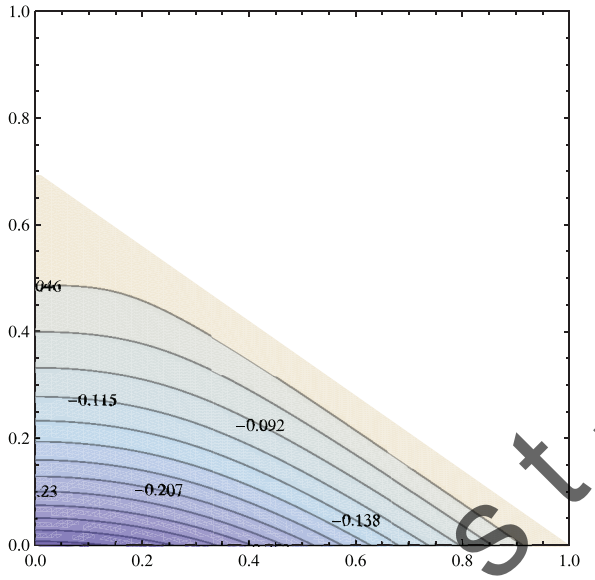

Fig. 11. Physical stress component $T_{(11)}$ as a function of θ_1, θ_2, for the first example: $\psi = 35^\circ$, and $\varphi = 35^\circ$. Contour plot of $T_{(11)}$ in the right hand side of the pile.

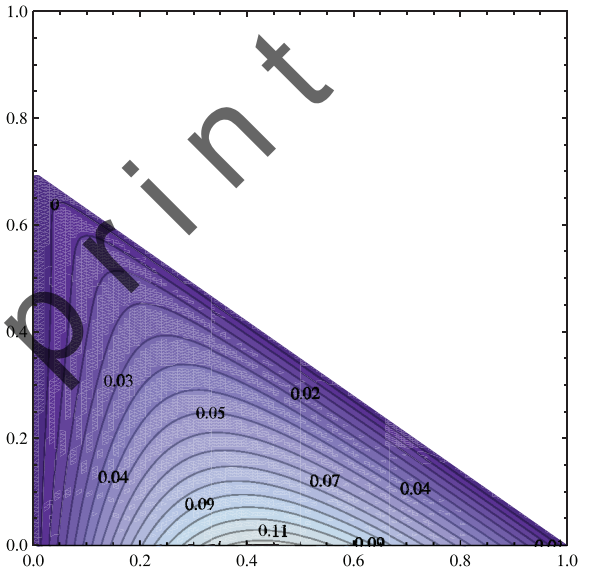

Fig. 12. Physical stress component $T_{(12)}$ as a function of θ_1, θ_2, for the first example: $\psi = 35^\circ$, and $\varphi = 35^\circ$. Contour plot of $T_{(12)}$ in the right hand side of the pile.

strictly positive all over the triangular domain. The value of it is rather large, being less than 0.1, only in a narrow band located in proximity of the free surface. Such a state of stress of lower potential energy with respect to the previous one, could be reached either perturbing the limit equilibrium of the first case with a small vibration, or directly by adopting a more dynamic way of construction, namely the construction from a line source.

In Fig. 10b the profile of the stresses $T_{(22)}$, $T_{(12)}$, and of the stress component $T_{(11)}$, emerging at the base of the pile is depicted. Notice that we adopted the sign convention for stress in the stress matrix, then the negative sign of the normal stress means that $T_{(22)}$ points upward, and the positive sign of the shear stress means that $T_{(12)}$ points toward the left.

A pronounced central dip can be seen in the graph representing the pressure at the base in this second example.

5. A second example

5.1. First case: $\psi = 35^\circ$, $\varphi = 35^\circ$, $k_1 = 0.116\ \rho g$, $k_2 = -0.104\ \rho g$, $k_3 = 0.220\ \rho g$

In this second numerical example we explore the case of a smaller friction angle. We first consider the case in which the angle of repose $\psi = 35^\circ$ and the friction angle φ coincides with ψ. By assuming $k_2 = -0.104\ \rho g$, $k_3 = 0.220\,\rho g$ and changing the value of the parameter $k_1/(\rho g)$ in the range [0, 1] we find that the stress satisfies the Mohr Coulomb constraint, in a narrow neighborhood around a single value of k_1, namely $k_1 = 0.116\ \rho g$. The results in terms of stress, corresponding to such a choice are summarized in Figs. 11–13, in a scale normalized by taking $\rho g = 1$, $a = 1$. In particular, in Fig. 11 the contour plot of the physical stress component $T_{(11)}$ is reported. Analogous plots of the shear component $T_{(12)}$ and of the normal component $T_{(22)}$ are depicted in Figs. 12 and 13.

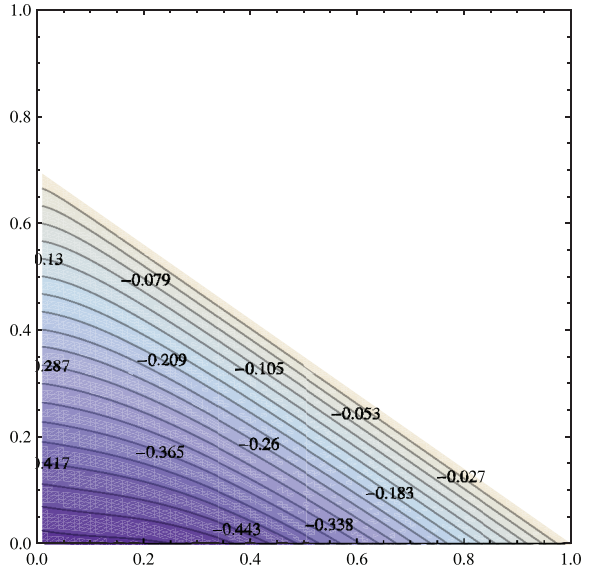

Fig. 13. Physical stress component $T_{(22)}$ as a function of θ_1, θ_2, for the first example: $\psi = 35^\circ$, and $\varphi = 35^\circ$. Contour plot of $T_{(22)}$ in the right hand side of the pile.

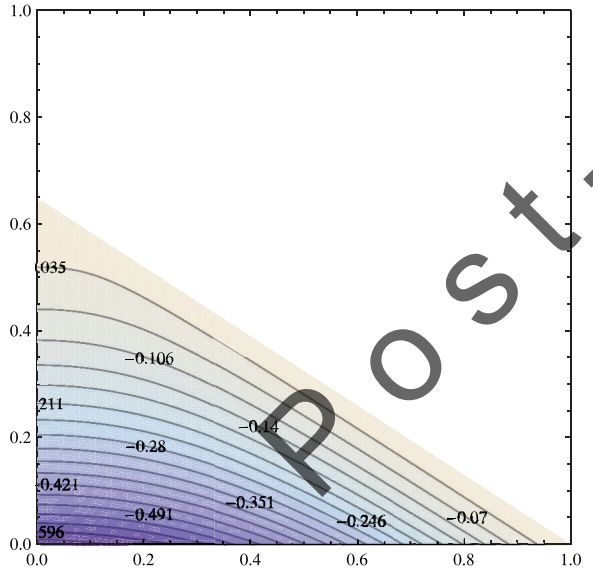

Fig. 14. Physical stress component $T_{(11)}$ as a function of θ_1, θ_2, for the second example: $\psi = 33^\circ$, and $\varphi = 35^\circ$. Contour plot of $T_{(11)}$ in the right hand side of the pile.

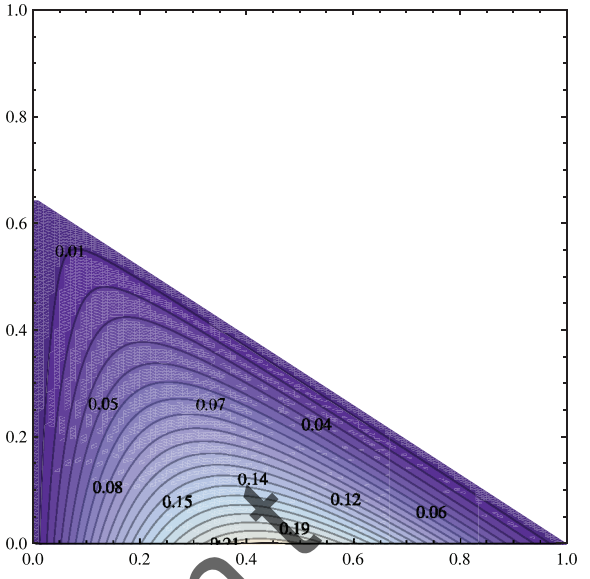

Fig. 15. Physical stress component $T_{(12)}$ as a function of θ_1, θ_2, for the second example: $\psi = 33^\circ$, and $\varphi = 35^\circ$. Contour plot of $T_{(12)}$ in the right hand side of the pile.

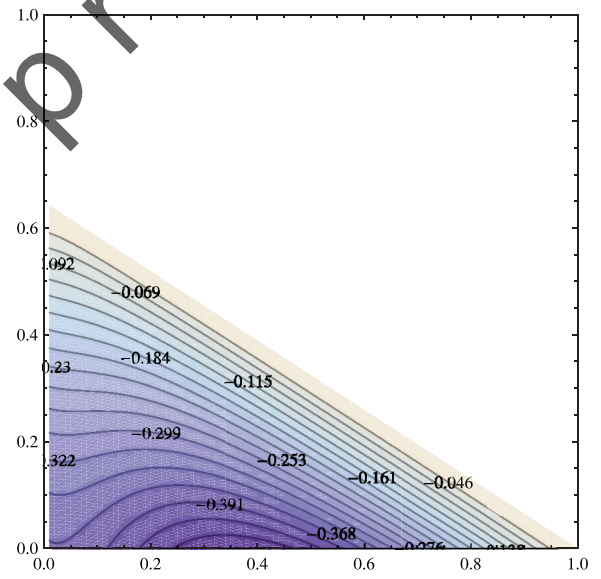

Fig. 16. Physical stress component $T_{(22)}$ as a function of θ_1, θ_2, for the second example: $\psi = 33^\circ$, and $\varphi = 35^\circ$. Contour plot of $T_{(22)}$ in the right hand side of the pile.

In Fig. 17a, the contour plot of the distance $d(\mathbf{T})$ introduced in (28) is represented. From such a plot we see that the yield function is positive all over the triangular domain, though the value of it is rather small being less than 10^{-1}, all over the domain.

In Fig. 18a the profile of the stresses $T_{(22)}$, $T_{(12)}$, and of the stress component $T_{(11)}$, emerging at the base of the pile is depicted. Notice that we adopted the sign convention for stress in the stress matrix, then the negative sign of the normal stress means that $T_{(22)}$ points upward, and the positive sign of the shear stress means that $T_{(12)}$ points toward the left.

5.2. Second case: $\psi = 33^\circ$, $\varphi = 35^\circ$, $k_1 = 0.08\ \rho g$, $k_2 = 0.12\ \rho g$, $k_3 = 0.22\ \rho g$

As a second case, we then consider $h = \arctan 33^\circ$, namely that the angle of repose is $\psi = 33^\circ$, whilst we assume for the friction angle $\varphi = 35^\circ$. The idea is that the pile has suffered a less smooth construction history, with the result that the angle of repose is less than the friction

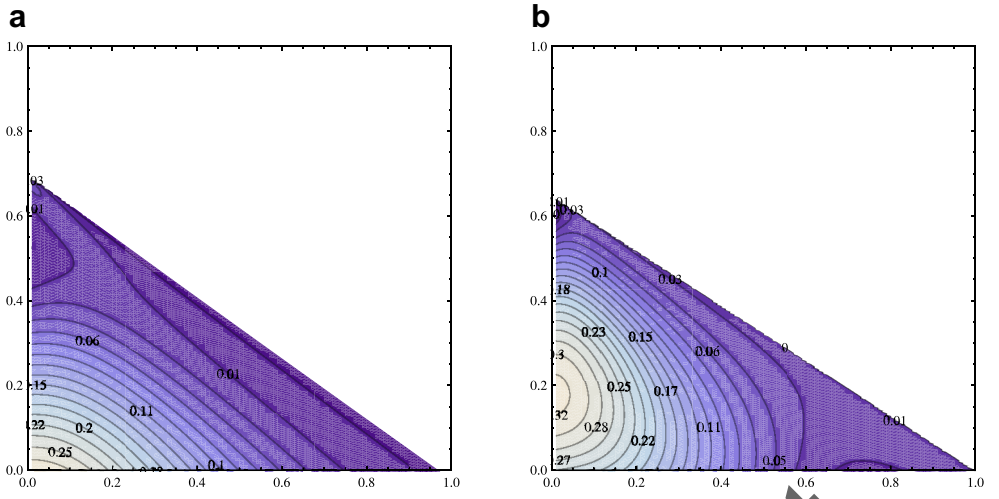

Fig. 17. Contour plot of $g = 1 - \cos^2(\varphi)(\mathrm{tr}\,\mathbf{T}/2)^2/\det\mathbf{T}$ as function of θ_1, θ_2, for the first (a) and the second (b) examples.

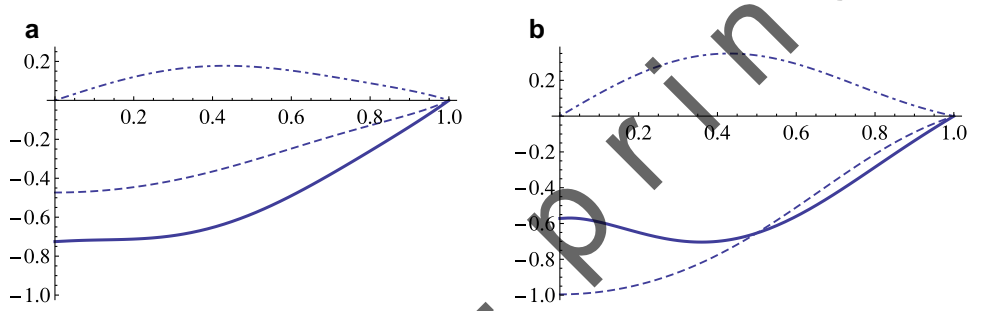

Fig. 18. Plot of the stress profiles at the base for the first (a) and the second (b) examples as functions of x_1, in the interval [0, a]. Dotted-dashed line: $T_{(12)}$, dashed line: $T_{(11)}$, solid line: $T_{(22)}$.

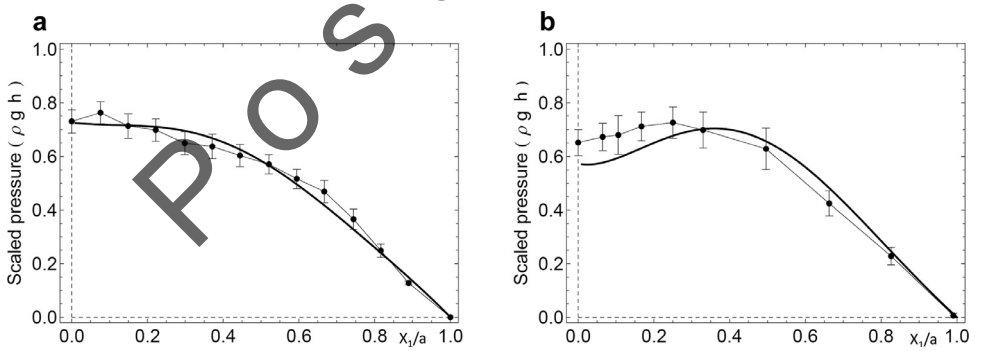

Fig. 19. Comparison of the stress profiles at the base corresponding two the first (a) and the second (b) analytical solutions, with the experimental results of Vanel et al. (1999).

angle. By assuming $k_2 = 0.12\ \rho g$, $k_3 = 0.22\ \rho g$ and changing the value of the parameter $k_1/(\rho g)$ in the range [0, 1] we find that the stress satisfies the Mohr Coulomb constraint, over an interval of values of k_1, whose maximum is $k_1 = 0.08\ \rho g$. The results in terms of stress, corresponding to such a choice are summarized in Figs. 14–16 in a scale normalized by taking $\rho g = 1$, $a = 1$. In particular in Fig. 14 the contour plot of the physical stress component $T_{(11)}$ is reported. Analogous plots of the shear component $T_{(12)}$ and of the normal component $T_{(22)}$ are depicted in Figs. 15 and 16.

In Fig. 17b, the contour plot of the distance $d(\mathbf{T})$ is represented. From such a plot we see that the yield function is strictly positive all over the triangular domain. The value of it is rather large, being less than 0.1, only in a narrow band located in proximity of the free surface. Such a state of stress of lower potential energy with respect to the previous one, could be reached either perturbing the limit equilibrium of the first case with a small vibration, or directly by adopting a more dynamic way of construction, namely the construction from a line source.

In Fig. 18b the profile of the stresses $T_{(22)}$, $T_{(12)}$, and of the stress component $T_{(11)}$, emerging at the base of the pile is depicted. Notice that we adopted the sign convention for stress in the stress matrix, then the negative sign of the normal stress means that $T_{(22)}$ points upward, and the positive sign of the shear stress means that $T_{(12)}$ points toward the left.

A pronounced central dip can be seen in the graph representing the pressure at the base in this second example.

6. Comparison with test results and conclusions

In Figs. 10 and 18 the profile of the normal stress at the base, predicted by our analysis, for the four cases studied in the previous section, is reported. Notice that the normal stress emerging at the base for the second case of both examples ($\psi = 45^\circ$ and $\varphi = 35^\circ$), shows a pronounced dip beneath the apex of the pile. Such a dip is not present in the first case. The results obtained in terms of base pressure with our theory, are compared with an experimental test reported in the literature, namely the test performed by Vanel et al. (1999). The results reported by Vanel et al. (1999) refer to the measurement of the base pressure of prismatic sand piles (composed of granular materials with a repose angle of approximately $\varphi = 35^\circ$), constructed with two deposition procedures: through uniform raining (a) and from a line source (b).

Deposition from a line source is intuitively more shaky than uniform raining, since, in pouring the material from a stationary line source, each element of sand arrives at the apex of the pile, rolls down the slope disturbing the other grains, and finally comes to rest and is finally buried.

This idea is confirmed by comparing the results of the experiments with our analytical results. In particular, the first case that we presented in the second example ($\psi = 35^\circ, \varphi = 35^\circ$), namely the state of stress close to the limit state all over the pile, is very well reproduced by the experimental case (a) (uniform raining), whilst the second case of the second example ($\psi = 33^\circ, \varphi = 35^\circ$) reproduces closely the experimental case (b) (line source). The comparison of the experimental results in terms of pressure measured at the base, with the base pressure corresponding to the two statically admissible solutions derived through our analysis, are reported in Fig. 19a and b.

Appendix A. Curvilinear coordinates in 2d

Let (θ_1, θ_2) be a curvilinear coordinate couple defined over the plane domain Ω, through the relation

$$\boldsymbol{x} = \widehat{\mathbf{x}}(\theta_1, \theta_2). \tag{A.1}$$

$\boldsymbol{x}$ being the position vector of a point of Ω.

The natural bases associated to the curvilinear lines $\{\theta_1, \theta_2\}$ are

$$\mathbf{a}_1 = \frac{\partial \boldsymbol{x}}{\partial \theta_1}, \qquad \mathbf{a}_2 = \frac{\partial \boldsymbol{x}}{\partial \theta_2}, \tag{A.2}$$

and the dual bases $\mathbf{a}^1$, $\mathbf{a}^2$, defined through the relation

$$\mathbf{a}^\alpha \cdot \mathbf{a}_\beta = \delta^\alpha_\beta, \tag{A.3}$$

δ^α_β being the Kronecker symbol, are

$$\mathbf{a}_1 = \frac{\partial \theta_1}{\partial x_\alpha}\,\widehat{\mathbf{e}}_\alpha, \qquad \mathbf{a}_2 = \frac{\partial \theta_2}{\partial x_\alpha}\,\widehat{\mathbf{e}}_\alpha, \tag{A.4}$$

The component forms of vectors and tensors in this curvilinear system and in the global Cartesian frame are

$$\begin{aligned} &\mathbf{u} = u^\alpha \mathbf{a}_\alpha = u_\beta \mathbf{a}^\beta = u_\gamma \widehat{\mathbf{e}}_\gamma, \\ &\mathbf{T} = T^{\alpha\beta}\mathbf{a}_\alpha \otimes \mathbf{a}_\beta = T_{\alpha\beta}\mathbf{a}^\alpha \otimes \mathbf{a}^\beta = T^\alpha_\beta \mathbf{a}^\alpha \otimes \mathbf{a}_\beta \\ &\quad = T_{(\alpha\beta)}\widehat{\mathbf{e}}_\alpha \otimes \widehat{\mathbf{e}}_\beta, \end{aligned} \tag{A.5}$$

where $\otimes$ denotes the tensor (dyadic) product. Such vector and tensor components can be obtained by other component forms through scalar products, namely

$$\begin{aligned} &u^\alpha = \mathbf{u}\cdot\mathbf{a}^\alpha, \quad u_\alpha = \mathbf{u}\cdot\mathbf{a}_\alpha, \quad u_\gamma = \mathbf{u}\cdot\widehat{\mathbf{e}}_\alpha, \\ &T^{\alpha\beta} = \mathbf{T}\cdot(\mathbf{a}^\alpha \otimes \mathbf{a}^\beta), \quad T_{\alpha\beta} = \mathbf{T}\cdot(\mathbf{a}_\alpha \otimes \mathbf{a}_\beta), \\ &T_{(\alpha\beta)} = \mathbf{T}\cdot(\widehat{\mathbf{e}}_\alpha \otimes \widehat{\mathbf{e}}_\beta). \end{aligned} \tag{A.6}$$

The gradient of a scalar field $\varphi(x)$ defined over Ω can be computed in curvilinear coordinates through the chain rule. Since

$$\mathrm{grad}\varphi(x) = \frac{\partial \varphi}{\partial x_\beta}\,\widehat{\mathbf{e}}_\beta \tag{A.7}$$

then

$$\mathrm{grad}\varphi(x) = \frac{\partial \varphi}{\partial \theta_\alpha}\,\frac{\partial \theta_\alpha}{\partial x_\beta}\,\widehat{\mathbf{e}}_\beta = \frac{\partial \varphi}{\partial \theta_\alpha}\,\mathbf{a}^\alpha \tag{A.8}$$

Analogously, if $\mathbf{u}$ is a vector field and $\mathbf{T}$ is a tensor field on Ω, the gradient and the divergence of the vector field $\mathbf{u}$ and the right divergence of the tensor field $\mathbf{T}$ are

$$\begin{aligned} &\mathrm{grad}\ \mathbf{u} = \frac{\partial \mathbf{u}}{\partial \theta_\alpha} \otimes \mathbf{a}^\alpha, \\ &\mathrm{div}\ \mathbf{u} = \frac{\partial \mathbf{u}}{\partial \theta_\alpha} \cdot \mathbf{a}^\alpha, \\ &\mathrm{div}\ \mathbf{T} = \frac{\partial \mathbf{T}}{\partial \theta_\alpha}\,\mathbf{a}^\alpha. \end{aligned} \tag{A.9}$$

References

Angelillo, M., 1993. Constitutive equation for no-tension materials. Meccanica 28 (2), 195–202.

Angelillo, M., Babilio, E., Cardamone, L., Fortunato, A., Lippiello, M., 2014. Some remarks on the retrofitting of masonry structures with composites. Composites B 61, 11–16.

Angelillo, M., Cardamone, L., Fortunato, A., 2010. A numerical model for masonry-like structures. J. Mech. Mater. Struct. 5, 583–615.

Angelillo, M., Fortunato, A., Fraternali, F., 2014. Structural capacity of masonry walls under horizontal loads. Ing. Sismica 1, 41–49.

Angelillo, M., Fortunato, A., Montanino, A., Lippiello, M., 2014. Singular stress fields in masonry walls: Derand was right. Meccanica 49 (5), 1243–1262.

Bierwisch, C., Kraft, T., Riedel, H., Moseler, M., 2009. Three-dimensional discrete element models for the granular statics and dynamics of powders in cavity filling. J. Mech. Phys. Solids 57, 10–31.

Chorin, A., Marsden, J., 2000. A Mathematical Introduction to Fluid Mechanics. Springer.

Dostal, Z., 2009. Optimal Quadratic Programming Algorithms: With Applications to Variational Inequalities, 1st edition Springer Publishing Company, Incorporated.

Fortunato, A., 2010. Elastic solutions for masonry-like panels. J. Elast. 39, 87–110.

Heyman, J., 1966. The stone skeleton. Int. J. Solids Struct. 2, 249–279.

Lippiello, M., 2007. Approximationof the quasi-static evolution of granular masses (Ph.D. thesis), Realprint s.r.l., Napoli.
Michalowski, R.L., Park, N., 2004. Admissible stress fields and arching in piles of sand. Geotechnique 54 (8), 529–538.
Michalowski, R.L., Park, N., 2004. Arching in granular media. In: Proceedings of ICTAM04, Warsaw, Poland.
Michalowski, R.L., Park, N., 2005. Arching in granular soils. In: Proceedings of the first Japan–U.S. Workshop on Testing, Modeling, and Simulation, vol. 143. ASCE Geotechnical Special Publication, pp. pp.255–268.
Pipatpongsa, T., Heng, S., Iizuka, A., Ohta, O., 2010. Statics of loose triangular embankment under Nadai's sand hill analogy. J. Mech. Phys. Solids 58, 1506–1523.
Pipatpongsa, T., Siriteerakul, S., 2010. Analytic solutions for stresses in conical sand heaps piled up with perfect memory. J. Appl. Mech. 13, 343–354.
Schechter, H., Bridson, R., 2012. Ghost SPH for animating water. ACM Trans. Graph. 31 (4), 61–68.
Sibille, L., Hadda, N., Nicot, F., Tordesillas, A., Darve, F., 2015. Granular plasticity, a contribution from discrete mechanics. J. Mech. Phys. Solids 75, 119–139.
Vanel, L., Howell, D., Clark, D., Behringer, R.P., Clement, E., 1999. Memories in sand: experimental tests of construction history on stress distributions under sandpiles. Phys. Rev. E 60 (5), 5040–5043.
Wittmer, J.P., Cates, M.E., Claudin, P., 1996. Stress propagation and arching in static sandpiles. J. Phys. I 7, 1–38.
Zhu, H.P., Zhou, Z.Y., Yang, R.Y., Yu, A.B., 2008. Discrete particle simulation of particulate systems: a review of major applications and findings. Chem. Eng. Sci. 63, 5728–5770.